Mon. Not. R. astr. Soc. (1981) **194**, 623–638

Power spectrum of small-scale density irregularities in the interstellar medium

J. W. Armstrong★ *National Radio Astronomy Observatory,† Green Bank, West Virginia, USA*

B. J. Rickett *Department of Electrical Engineering and Computer Science, University of California, La Jolla, California, USA*

Received 1980 July 2; in original form 1980 May 22

Summary. Interstellar scintillation (ISS) observations of 17 pulsars are used to place new limits on the spectrum of small-scale electron density irregularities in the interstellar medium. The time-dependent radio frequency spectrum of ISS is the observed quantity; from this we determine the ISS scintillation index (rms intensity/mean intensity) and a precisely defined ISS frequency-correlation scale based on the autocorrelation function in radio-frequency of the ISS fluctuations. Measurements were made at 340, 408 and 450 MHz and in the dispersion measure range 3–57 cm^{-3} pc. Limits to the scintillation parameters were obtained for pulsars with $89 \leqslant DM \leqslant 158$ cm^{-3} pc. The observations are compared with model interstellar medium spectra of the power-law form (spectrum proportional to wavenumber$^{-\alpha}$, $2 \leqslant \alpha \leqslant 4$) and the Gaussian (or square-law structure function) form. The dispersion-measure dependence of the ISS frequency-correlation scale, B, is consistent with either the Gaussian model or power-law models having $3.0 \lesssim \alpha \leqslant 4$. Although data were taken over only a limited range of centre frequencies, the radio-frequency scaling of B is consistent with power-law models having $2.8 \lesssim \alpha \lesssim 3.9$. However, by comparing the shape of the radio-frequency autocorrelation function with model (thin screen) calculations, we only find good agreement with power-law models having large ($\alpha \gtrsim 3.6$) spectral indices. Our data are consistent with the level of the local three-dimensional density spectrum at $q = 10^{-9}$ m^{-1} of 3×10^{28} to 3×10^{29} m^{-3}.

1 Introduction

Radio-wave scattering by interstellar electron density irregularities produces a number of observable phenomena. Among these phenomena are the temporal broadening of pulses,

★ Present address: Jet Propulsion Laboratory, California Institute of Technology, 4800 Oak Grove Drive, MS 238-737, Pasadena, California 91103, USA.

† Operated by Associated Universities, under contract with the National Science Foundation.

angular broadening of radio sources, and intensity fluctuations (interstellar scintillation – ISS) having fine structure in time and radio frequency. Interstellar scattering can be used to study the small-scale turbulence in the interstellar medium (ISM) and is also relevant to pulsar studies (Rankin *et al.* 1970; Lang 1971), continuum source investigations (Condon & Backer 1975; Armstrong, Spangler & Hardee 1977; Condon & Dennison 1978; Cordes & Dickey 1979), and galactic cosmic-ray confinement studies (Cesarsky 1980). It should be noted that the electron density fluctuations relevant to ISS may or may not be strictly 'turbulent' (i.e. characterized by diffusivity, three-dimensional vorticity fluctuations and energy transfer from large to small eddies). However, it is convenient (and conventional in scintillation studies) to refer to the ISM fluctuations as 'turbulent'.

The primary source of information on the small-scale ($\sim 10^9$ m) ISM turbulence has come from observations of pulsars. Pulse broadening is most readily interpreted in principle, but it can be studied only for those few (heavily scattered) pulsars for which the broadening time is much longer than the average pulse width. ISS observations made on a larger number of pulsars have been used to estimate the characteristic scales of the scintillation pattern in time ($\sim 10^2$–10^4 s), in frequency ($\sim$ kHz to MHz), and in a few cases in spatial extent ($\sim 10^4$ km). However, most of these estimates (e.g. Rickett 1970; Lang 1971) have been based on rather crude data processing yielding a single parameter (e.g. frequency scale) with large estimation errors. The basic difficulty centres on the slow nature of ISS, requiring many hours of observations for only 1–100 independent intensity estimates at a single frequency. In a recent paper Roberts & Ables (1980) have made a comprehensive study of the ISS from the stronger pulsars visible from Australia. They present careful measurements of the frequency and time variations using multiple filter banks over a range of centre frequencies.

In this paper we report observations of the ISS radio spectrum over up to 10 MHz. The data have been processed carefully to account for instrumental resolution and system noise. The power spectrum of the ISM irregularities is the quantity of main physical interest, and our goal is to determine – or provide useful limits to – the ISM power spectrum in the range of scale sizes relevant to ISS. The interpretation of the observations involves (1) precisely defining an ISS frequency scale and determining its dependence on dispersion measure and radio frequency, (2) measuring of the scintillation index (= rms intensity/mean intensity), and (3) determining the shape of the autocorrelation of the ISS radio-frequency spectrum. We compare our results with those of Roberts & Ables (1980).

2 Theory

The theory of ISS intensity fluctuations in space and radio frequency has been reviewed by Rickett (1977); the reader is referred to that article for the primary theoretical references. In this section we merely summarize results relevant to our present observations. The notation follows that of Rickett (1977). The z-axis is the direction of propagation.

The ISM electron density fluctuations are assumed 'weak' (so that deviations are small compared with the mean value), on scales large compared with the radio wavelength, and characterized by a (three-dimensional) correlation function $R_N(\mathbf{r}; z') = \langle n(\mathbf{r}')\, n(\mathbf{r}'+\mathbf{r})\rangle$ where $n(\mathbf{r})$ is the deviation of the electron density from the mean and $\mathbf{r} = (x, y, z)$. (The explicit dependence of R_N on z' allows for a possible slow dependence on position, assumed separable.) The Fourier transform of R_N is the spatial wavenumber spectrum M_{3N}. We consider only two idealized models for M_{3N}. These are the power-law spectrum

$$M_{3N}(q_x, q_y, q_z) = C_N^2(z') \cdot [q_x^2 + q_y^2 + q_z^2 + \kappa_1^2]^{-\alpha/2} \qquad (1)$$

and the Gaussian spectrum

$$M_{3N}(q_x, q_y, q_z) = G_N^2(z') \exp\left[-\frac{q_x^2 + q_y^2 + q_z^2}{\kappa_0^2}\right]. \quad (2)$$

The wavevector (q_x, q_y, q_z) is the transform variable conjugate to $\mathbf{r}$; G_N^2 and C_N^2 measure the 'level' of the turbulence; $2\pi/\kappa_0$ is a typical blob size in the Gaussian model; and $2\pi/\kappa_1$ is the 'outer scale' in the power-law model. The Gaussian spectrum models a situation where there is a discrete scale in the range of scales to which the observations are sensitive. For example, this discrete scale might be associated with a dominant plasma instability or an 'inner scale' of broadband turbulence extending to wavenumbers lower than can be measured with ISS. The Gaussian model can also be called a 'square-law structure function' model since, for $(x^2 + y^2)^{1/2} \ll \kappa_0^{-1}$, the transverse structure function of the irregularities depends quadratically on the separation. The power-law model spectra are idealizations of broadband fluctuations. For $\alpha = 11/3$, equation (1) corresponds to the Kolmogorov inertial subrange which has proven useful in the description of neutral turbulence and the characterization of large-scale plasma irregularities in the solar wind outside the acceleration region (e.g. Woo & Armstrong 1979). For $2 < \alpha < 4$ and separations small compared with κ_1^{-1}, the transverse structure function is proportional to $(x^2 + y^2)^{(\alpha-2)/2}$ so that the $\alpha = 4$ model is also a 'square-law structure function' model. For $\alpha > 4$, the structure function depends on κ_1 but also takes a square-law dependence on separation. Thus all $\alpha \geqslant 4$ will be included with the Gaussian model under the heading of square-law structure function. All subsequent power-law formulae are restricted to $2 < \alpha < 4$.

The observable quantity in our investigation is the fluctuation of pulsar intensity over radio frequency and time (on time-scales long compared with the pulse period). Let $I(\omega, \mathbf{s})$ be the intensity fluctuation at angular radio frequency ω and position $\mathbf{s} = (x, y)$ in the transverse plane. The mean (averaging time long compared with the pulse period but short compared to 'secular' changes in the pulsar intensity) is taken to be unity. The space–frequency autocorrelation function characterizes the statistics of $I(\omega, \mathbf{s})$:

$$\gamma_4(\Delta\omega, \mathbf{s}; \omega_0) \equiv \langle I(\omega_0, \mathbf{s}')\, I(\omega_0 + \Delta\omega, \mathbf{s}' + \mathbf{s})\rangle, \quad (3)$$

where $\Delta\omega \ll \omega_0$, the centre frequency. The connection between γ_4 and M_{3N} depends on the strength of the scattering, U. U is defined as the square of the scintillation index as calculated according to the Born approximation. Thus U is precisely defined in both weak and strong scattering even though the Born approximation only applies when $U \ll 1$ (Rumsey 1975). If $U \ll 1$, γ_4 and M_{3N} are related by equation (37) of Rickett (1977) and $m^2 \ll 1$, where m is the observed (point source) scintillation index. For $U \gg 1$, $m \to 1$ regardless of the spatial power spectrum and

$$\gamma_4(\Delta\omega, \mathbf{s}; \omega_0) \approx |\gamma_2(\Delta\omega, \mathbf{s}; \omega_0)|^2, \quad (4)$$

where $\gamma_2(\Delta\omega, \mathbf{s}; \omega_0) = \langle u(\omega_0, \mathbf{s}')\, u^*(\omega_0 + \Delta\omega, \mathbf{s}' + \mathbf{s})\rangle$, and $u(\omega, \mathbf{s})$ is the complex Fourier component of the electric field at position $\mathbf{s}$. Differential equations for the propagation of γ_2 can be written (Lee 1974). For the power-law models of the extended medium these must be solved numerically (Lee & Jokipii 1975); for the Gaussian model with uniform extended turbulence an analytic solution has been found (Chashei & Shishov 1976; Lerche 1979). For the $U \gg 1$ limit of interest here, Lovelace (1970) obtained the following results

for $\gamma_4 = |\gamma_2|^2$ for a thin layer of turbulence and an incident plane wave:

$$\gamma_4(\Delta\omega, 0) \cong \begin{cases} \dfrac{1}{1 + (\text{const. } \Delta\omega/\omega)^2} \text{ (Gaussian)} & (5) \\ \left| i \displaystyle\int_0^{+\infty} dx \exp\left[-(\text{const. } \Delta\omega/\omega x)^{\alpha-2/2}\right] \exp(ix) \right|^2. \text{ (Power law)} & (6) \end{cases}$$

These equations (5) and (6) can be used to produce model frequency-autocorrelation functions for comparison with the data. A comparison of the thin-screen plane-wave result (equation 5) with the extended Gaussian turbulence model (Chashei & Shishov 1976) is given in Appendix 1. We take the ISS frequency scale, B, to be the half-width to e^{-1} of $\gamma_4(f)$.

For $U \gg 1$ and if the ISM is statistically homogeneous, B should scale with propagation distance z and centre frequency of observation according to $B \propto z^{-2}\omega^{+4}$ (Gaussian) or $B \propto z^{\alpha/(2-\alpha)}\omega^{2\alpha/(\alpha-2)}$ (power-law). A noteworthy property of the $(2 < \alpha < 4)$ power-law model, however, is that it cannot give a correlation bandwidth B small compared with the centre frequency if $U \ll 1$. Thus observations showing $m < 1$ (i.e. $U \ll 1$) with $B \ll \omega/2\pi$ would be sufficient to exclude such power-law models.

Finally, it is useful to consider the temporal Fourier transform of γ_4, defined by

$$\tilde{\gamma}_4(\tau, 0) = (2\pi)^{-1} \int_{-\infty}^{+\infty} \exp\left[i\tau(\Delta\omega)\right] \gamma_4(\Delta\omega, 0)\, d(\Delta\omega). \quad (7)$$

This quantity can be interpreted as the autocorrelation function of the pulse-broadening function. Alternatively, $\tilde{\gamma}_4(\tau)$ is a 'fluctuation power spectrum' which shows how the variance of $I(\omega, 0)$ is decomposed over fluctuation 'frequency' (cycle Hz^{-1}). This second interpretation is useful in considering instrumental biases introduced into estimates of $\gamma_4(\Delta f)$ and hence B.

3 Observations and data analysis

The observations were made in 1976 March using the National Radio Astronomy Observatory's 91-m telescope. The signals from orthogonal linearly polarized feeds were combined to give left- and right-circular polarized signals. These were passed through standard 250–500 MHz preamplifiers, mixed to 30 MHz, and fed to the Model III spectrometer (Shalloway, Mauzey & Greenhalgh 1972). The Model III receiver is a one-bit autocorrelation spectrometer with auxiliary total-power counters for each input channel. The spectrometer can separately accumulate 'signal' and 'reference' spectra (with and without periodically added noise calibrations), with the reference spectra used to calibrate the system passband response. For our observations, signal and reference spectra were accumulated during time windows synchronized with the apparent (Doppler corrected) pulse period. Each pulsar was tracked for ~ 40 min with the telescope's travelling feed, and the pulse phase determined from a signal averager connected to one polarization channel. The autocorrelator's signal window was set to be typically 50 per cent longer than the pulse duration times given by Taylor & Manchester (1975) and checked for synchronization with the pulse phase throughout each track. The signal and reference spectra were accumulated by the on-line data-logging computer for about 10 s, then written on to magnetic tape along with total power and timing information for later processing. Usually spectra were obtained simultaneously at different frequency resolutions in the two orthogonal polarizations. The pairs of total rf bandwidths analysed were usually 10 MHz/1.25 MHz, 2.5 MHz/312.5 kHz, or 1.25 MHz/156.25 kHz with

each bandwidth pair centred on the same radio frequency. Operated in this mode, the Model III receiver gives 192 channels per polarization. When scheduling permitted, observations were made at centre frequencies of 340, 408 and 450 MHz.

In the subsequent processing, the signal and reference spectra were accumulated for 30–60 s and the quotient spectrum $I(f) \equiv$ [(signal spectrum − reference spectrum) × system temperature/reference spectrum] was formed. Figs 1–3 show time-dependent rf spectra determined by this procedure; the changing fine structure due to ISS is clearly evident. Intrinsic pulse-to-pulse fluctuations are effectively suppressed by the 30–60 s coherent integration. In addition, such intrinsic fluctuations are thought to be broad-band, so that the fine structure in these spectra are due to ISS. (They could in principle include a narrow-band intrinsic fluctuation if such a process exists, as discussed by Roberts & Ables 1980.) Whereas the spectra in Fig. 3 are evidently random in appearance, the spectra in Fig. 2 (and to a much lesser extent in Fig. 1) show ISS signals apparently systematically drifting in frequency-time. Roberts & Ables (1980) and Hewish (1980) have discussed such features at some length; we will not pursue them here as they were only clearly observed for PSR 1133+16. A further difference from the work of Roberts & Ables comes from our use of a digital spectrometer so that inter-channel coupling is precisely known – see Appendix 2 for details.

The quantity of main interest is $\gamma_4(\Delta f) = \gamma_4(2\pi\Delta f, 0; \omega_0)$ as defined by equation (3). We did not compute γ_4 from the lagged product definition, equation (3), but rather from the inverse Fourier transform of $\langle |\tilde{I}(\tau)|^2 \rangle$, where $\tilde{I}(\tau)$ is the Fourier transform of each quotient spectrum, $I(f)$. This approach was used because it is computationally efficient and because it allows the intermediate result, $\tilde{\gamma}_4$, to be studied for instrumental effects and

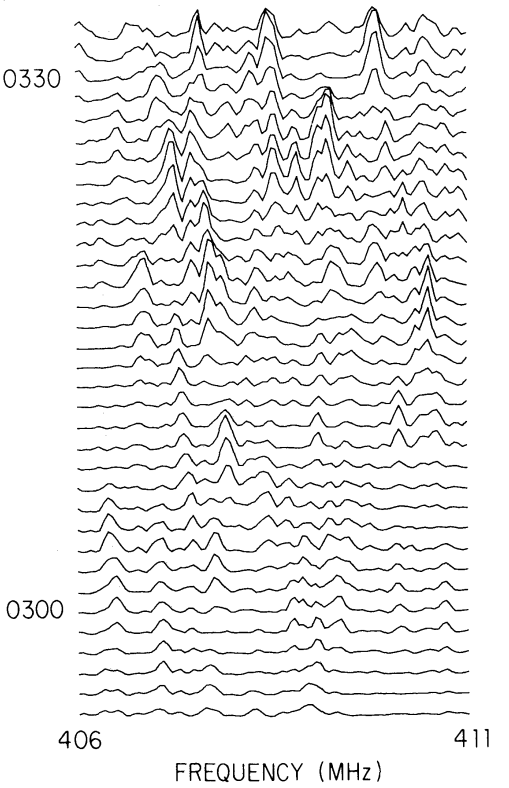

Figure 1. Radio-frequency spectrum of ISS as a function of time. Time increases to top of figure; vertical scale is linear. Source is PSR 0329+54. Data taken more than about 20 min from meridian transit are suppressed by the antenna power pattern.

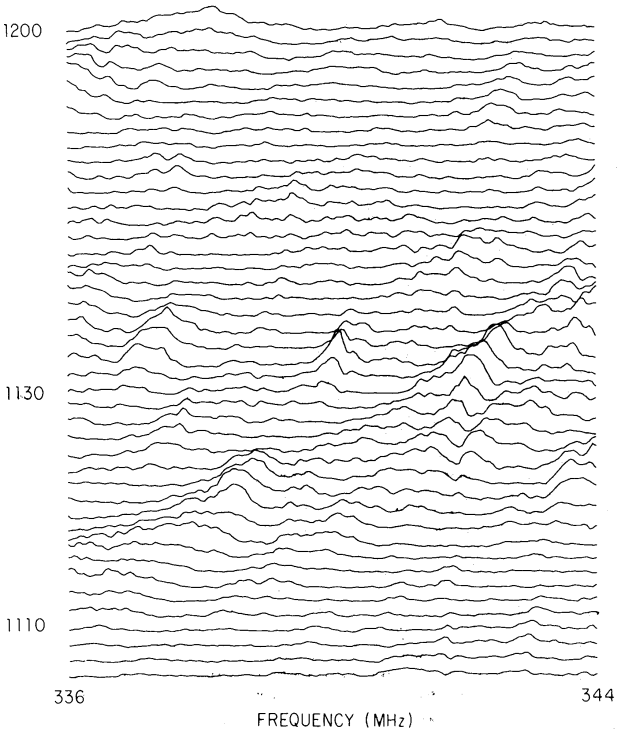

Figure 2. As Fig. 1, for PSR 1133+16.

system noise. The $\tilde{\gamma}_4(\tau) \equiv \langle |\tilde{I}(\tau)|^2 \rangle$ were formed in accordance with procedures recommended by Jenkins & Watts (1968): the data series $I(f)$ was 'prewhitened' by a first-difference filter, Fourier transformed, squared, averaged, and then 'post-darkened' by correcting for the transfer function of the difference filter. Before doing the inverse transform to get

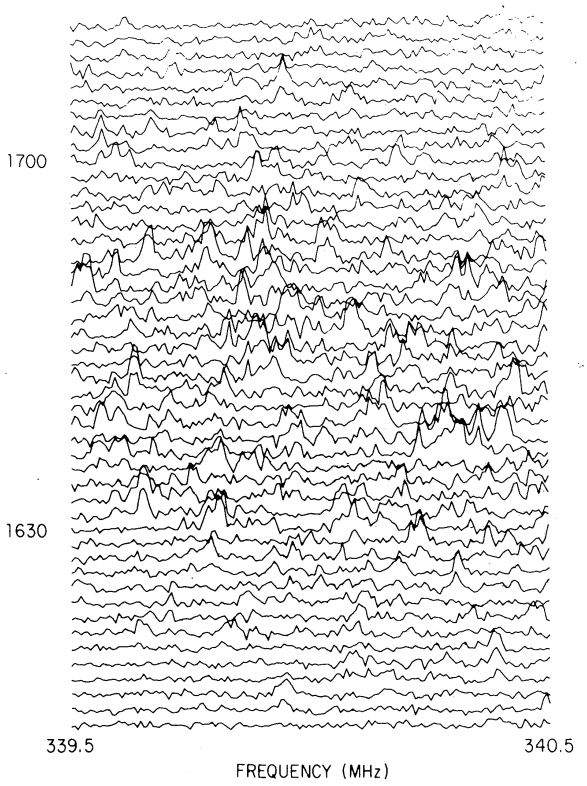

Figure 3. As Fig. 1, for PSR 1642-03.

$\gamma_4(\Delta f)$, the Fourier components at $\tau = 0$ and $\tau =$ (total rf bandwidth)$^{-1}$ were inserted by extrapolating a linear fit to the small τ components of $\tilde{\gamma}_4(\tau)$. The observed $\tilde{\gamma}_4(\tau)$ contained a 'white noise' component at large τ, associated with the system noise. This noise level was estimated and subtracted from $\tilde{\gamma}_4$ before the inverse Fourier transformation gave γ_4. (This was done to get an unbiased estimate of γ_4 for the ISS process alone, rather than the sum of the ISS process and the system noise fluctuations.) The correlation bandwidth, B, was estimated as the half-width to e^{-1} of $\gamma_4(\Delta f)$. As discussed in Appendix 2, no correction for the resolution function of the spectrometer is necessary.

For the stronger pulsars, reliable estimates of both the pulsar flux (averaged over ~1 min) and the ISS fluctuation power could be made. The scintillation index, m, of the ISS was then computed according to

$$m^2 = 2\langle I\rangle^{-2} \int_{\tau_{\min}}^{\tau_{\max}} d\tau \, [\langle |\tilde{I}(\tau)|^2\rangle - N] \,, \tag{8}$$

where $\langle I\rangle$ is the estimated mean flux and N is the 'white noise level'. The largest τ, $\tau_{\max}$, is related to the resolution of the spectrometer, δf, by $\tau_{\max} = 1/(2\delta f)$. The smallest τ, $\tau_{\min}$, is set by the reciprocal of the total rf bandwidth analysed. Clearly Fourier components of I having 'fluctuation frequencies' smaller than $\tau_{\min}$ are not measured and cannot contribute to the observed scintillation index.

4 Results

Fig. 4 shows examples of $\gamma_4(\Delta f)$ and $\tilde{\gamma}_4(\tau)$. It is noteworthy that for many of our observations $\tilde{\gamma}_4(\tau)$ is approximately a power-law function of τ over the range of τ's to which the observation was sensitive, e.g. Fig. 4(b) and (c). In these cases the ISS correlation bandwidth is not resolved, since it is greater than or approximately equal to the total rf bandwidth analysed. In such cases, we take the $1/e$ halfwidth of the observed $\gamma_4(\Delta f)$ as a lower limit to the true ISS correlation bandwidth. It should be noted that in these cases the observed scintillation index is expected to be a systematic underestimate of the true scintillation index, since the entire scintillation spectrum, $\tilde{\gamma}_4$, is not measured.

4.1 SCINTILLATION INDEX

The observed scintillation index results are given in Table 1. When B is not resolved, the observed index is entered as a lower limit. When B is resolved $m \approx 1$, consistent with either the Gaussian or power-law models in the $U \gg 1$ limit.

4.2 CORRELATION BANDWIDTH

The measured correlation bandwidths are also listed in Table 1. Again, if B is under-resolved the observed $1/e$ halfwidth of γ_4 is entered as a lower limit. For some of the high-dispersion-measure pulsars, we did not detect ISS. That is, a plot of $\tilde{\gamma}_4(\tau)$ did not clearly show a 'small τ excess' above the system noise. In these cases we calculated an approximate limit to the ISS correlation bandwidth as follows. Assuming $m = 1$ and taking the 408-MHz average pulse energy from Taylor & Manchester (1975), we obtained an estimate of the variance of the ISS process (at 408 MHz). For the Gaussian model we could then calculate the value of B that would cause the peak value of $\tilde{\gamma}_4$ to be 6 dB above the 'white noise level', N. (Small B causes wide $\tilde{\gamma}_4$ and – since the integral of $\tilde{\gamma}_4$ is fixed to be the variance of the ISS – makes the clear detection of small τ excess more difficult.)

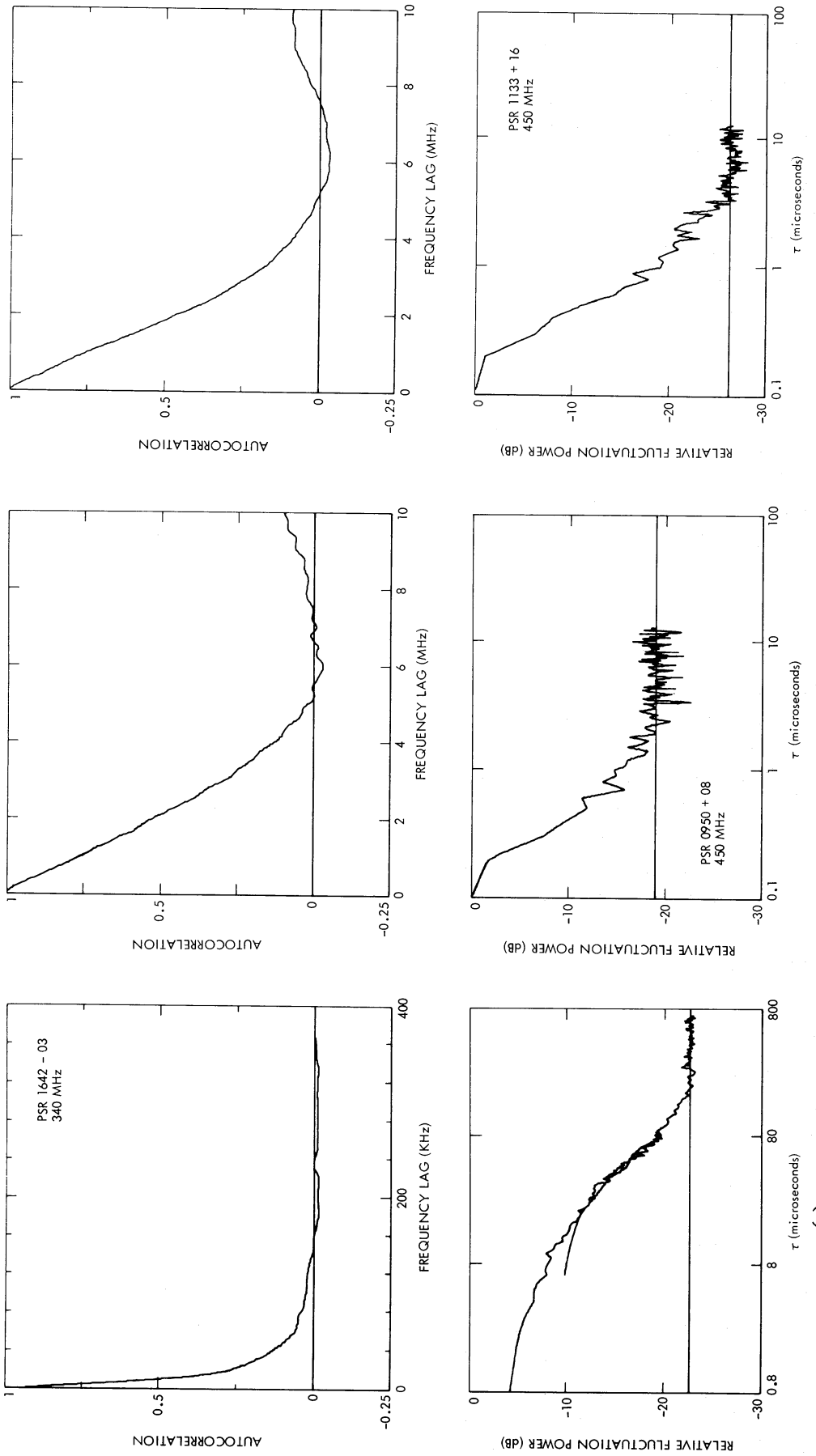

Figure 4. Examples of radio-frequency autocorrelation functions, $\gamma_4(\Delta f)$, and their Fourier transforms, $\tilde{\gamma}_4(\tau)$. (a) PSR 1642 – 03, centre frequency 340 MHz, rf bandwidths analysed 1.25 MHz and 156.25 kHz, (b) PSR 0950 + 08, centre frequency 408 MHz, total rf bandwidth analysed 10 MHz, (c) PSR 1133 + 16, centre frequency 450 MHz, total rf bandwidth analysed 10 MHz.

1981MNRAS.194..623A

Table 1

PSR	*DM* (cm^{-3} pc)	*f* (MHz)	*B* (kHz)	*m*	Days observed	Comment
0329+54	26.8	340	36	0.97	1	very high SNR; 408 MHz observations give *B* range of 81–94 kHz, *m* in range of 1.02–1.04
		408	88	1.03	2	
0355+54	57.0	408	29	–	4	individual days have low SNR
0450 – 18	39.9	408	142	0.85	1	
0611+22	96.7	408	$\lesssim$40	–	2	no detection of ISS (see text)
0950+08	3.0	340	>1440	>0.43	5	range of daily *B* lower limits is 1210–2700 kHz (340 MHz) and 1270–3510 kHz (408 MHz)
		408	>2650	>0.29	4	
		450	>1750	>0.27	1	
1133+16	4.8	340	590	0.91	5	340 MHz data barely resolved
		408	>970	>0.82	4	
		450	>1520	>0.55	1	
1237+25	9.3	340	>670	>0.47	4	340 MHz data appears nearly resolved
		408	>990	>0.39	3	
1508+55	19.6	340	220	–	2	weak signal
		408	>366	–	1	
1642 – 03	35.7	340	11	0.89	6	*B* well-resolved
		408	43	1.19	3	
		450	61	–	1	
1907+10	144	408	$\lesssim$6	–	3	
1911 – 04	89.4	408	$\lesssim$9	–	6	no detection of ISS (see text)
1933+16	158.5	408	$\lesssim$3	–	3	
1946+35	129.1	408	$\lesssim$11	–	6	
2020+28	24.6	408	560	–	3	individual days have low SNR
		450	>830	–	4	
2045 – 16	11.5	340	>730	>0.24	1	
		408	>1130	>0.40	3	
		450	>1450	>0.39	4	
2217+47	43.5	408	56	–	5	individual days have low SNR
2303+30	49.9	408	87	–	3	individual days have low SNR

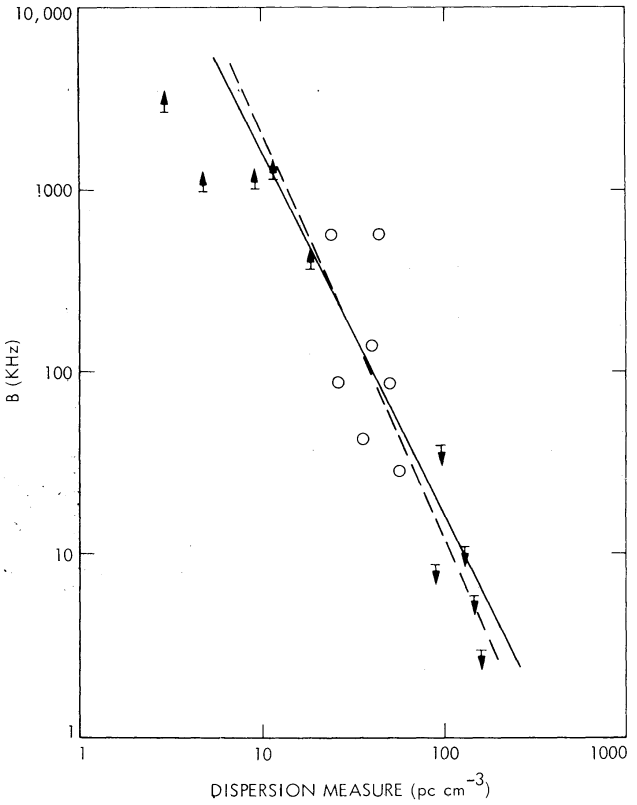

Figure 5. Plot of $1/e$ halfwidth of $\gamma_4 (\equiv B)$ versus dispersion measure for observations at 408 MHz. Solid and dashed lines have logarithmic slopes of -2 (Gaussian model) and -2.2 (Kolmogorov model).

Fig. 5 shows a plot of B (at 408 MHz) versus dispersion measure. It is clear that functional dependences of the form $B \propto DM^{-x}$ with $x \geqslant 2$ are consistent with these observations (although see Sutton (1971) and Rickett (1977) for a discussion of observations taken at large DM), so this dispersion-measure dependence is consistent with either the Gaussian or power-law models.

For only two pulsars (0329+54 and 1642–03) do we have resolved measurements of B at two or more frequencies. Although the frequency dependence of B on single objects is attractive as a way of determining power-spectrum model parameters along particular lines of sight, the uncertainties in the observed values of B are too large (considering the small frequency-separation) to constrain the radio-frequency scaling of B very severely. The 0329+54 data between 340 and 408 MHz give $B \propto f^{+4.9 \pm 0.8}$, corresponding to power-law indices $\alpha = 3.4$ (+0.5, −0.3). Similarly, for PSR 1642−03, $B \propto f^{5.6\,(+1.8,-1.3)}$ yielding $\alpha = 3.1$ (+0.7, −0.3). In computing the above uncertainties we have used the actual variation of our daily estimates of B as a measure of the statistical reliability or, in the case of single observations, we have used an uncertainty of ±7 per cent for these high signal-to-noise ratio data. The B values for 1642−03 are close to those obtained by Roberts & Ables (1980) – our only pulsar common to their study. In comparing results it must be noted that our definition of B is at a correlation of $1/e$ while theirs is at a value of 0.5.

4.3 γ_4 SHAPE

The shape of γ_4 (or $\tilde{\gamma}_4$) depends on the ISM power spectrum. Here we compare the observations with computed models based on thin-screen scattering and an incident plane

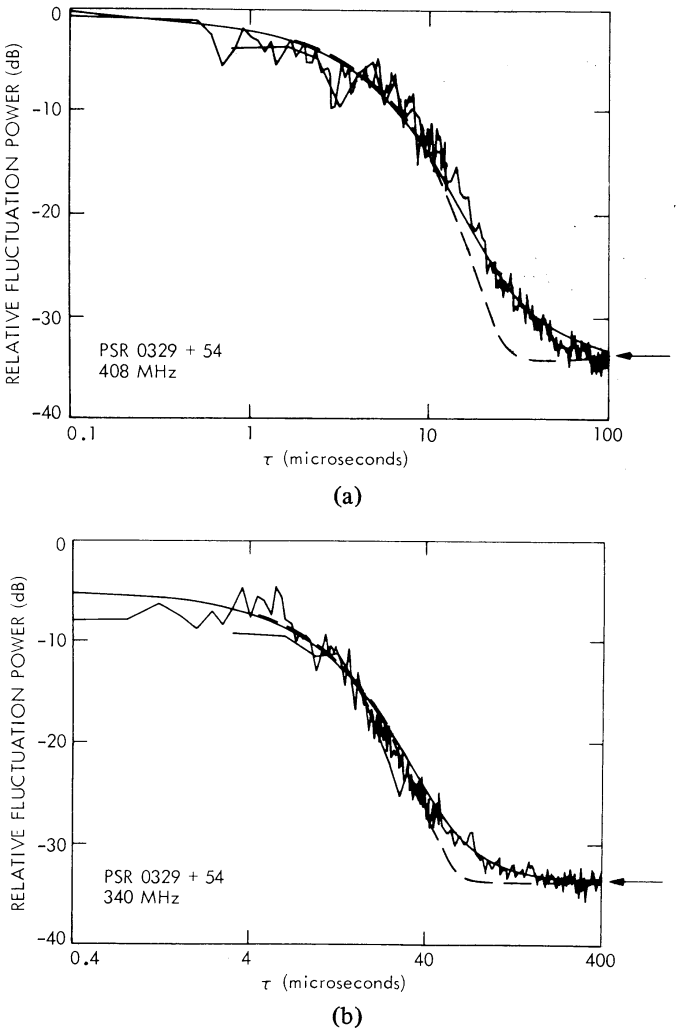

Figure 6. 'Fluctuation power spectra', $\tilde{\gamma}_4(\tau)$, for PSR 0329+54. (a) Centre frequency 408 MHz, bandwidths analysed 10 MHz and 1.25 MHz. (b) Centre frequency 340 MHz, bandwidths analysed 2.5 MHz and 312.5 kHz. Overplotted models are for the $\alpha = 3.9$ power law (solid lines) and Gaussian model (dashed lines).

wave (Lovelace 1970; our equations (5) and (6)). A partial justification for this approach is given in Appendix 1. We make the shape comparison in terms of $\tilde{\gamma}_4$, rather than γ_4, because $\tilde{\gamma}_4$ is non-committal regarding fluctuation 'frequencies' (cycles Hz^{-1}) not actually resolved.

Fig. 6 shows $\tilde{\gamma}_4$ for PSR 0329+54 at 408 and 340 MHz, along with the model calculation for the $\alpha = 3.9$ power law. Each overplotted model has the same area as the ISS signal component of the observed γ_4, (i.e. $\tilde{\gamma}_{4,\text{model}}(0) = \tilde{\gamma}_{4,\text{obs}}(0)$), the same B, and a noise level indicated by an arrow on the right has been added to the model before overplotting. No attempt has been made to make the correlation bandwidths of the two models obey the $f^{4.1}$ scaling predicted by the $\alpha = 3.9$ model. The fits seem remarkably good considering the simplicity of the model. Comparable goodness-of-fit can be obtained only for the large $\alpha(> 3.7)$ power laws. The Gaussian model is plotted as a dashed line and fits satisfactorily for the upper 15 dB, but is too 'convex' to fit the entire range. By reference to Appendix 1 it is clear that an extended-medium calculation would if anything worsen the fit, since the extended model is more 'convex' than the screen model plotted in Fig. 6. The disagreement

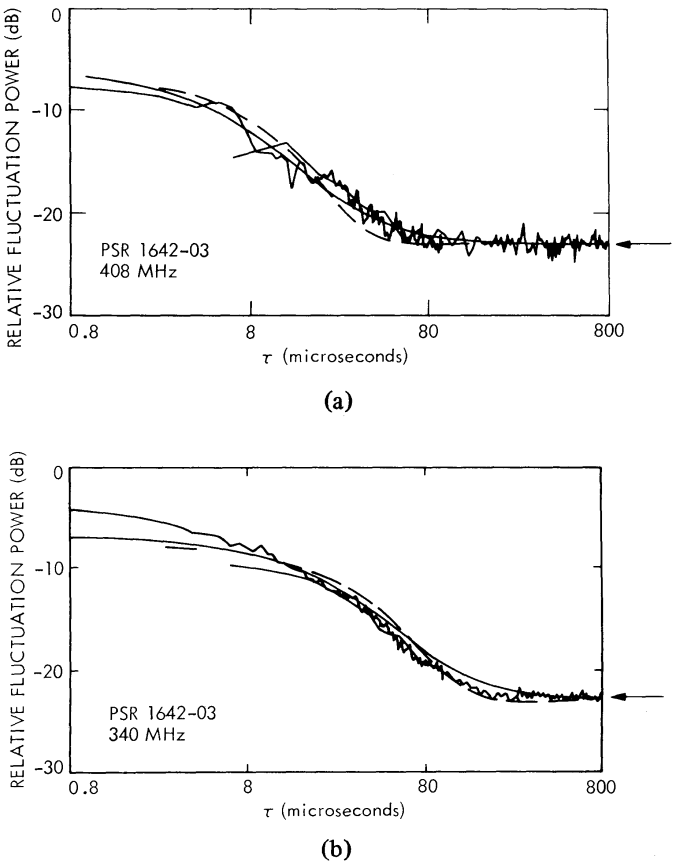

Figure 7. 'Fluctuation power spectra', $\tilde{\gamma}_4(\tau)$, for PSR 1642−03. (a) Centre frequency 408 MHz, bandwidths analysed 1.25 MHz and 156.25 kHz. (b) Centre frequency 340 MHz, bandwidths analysed 1.25 MHz and 156.25 kHz. Overplotted models are for the $\alpha = 3.6$ power law (solid lines) and Gaussian model (dashed lines).

with the Gaussian model is really only apparent with the large (> 30 dB) signal-to-noise ratio of these data.

Fig. 7 shows similar plots for PSR 1642-03. Here the signal-to-noise ratios are considerably smaller (about 15 dB) than those associated with 0329+54. The overplotted models are for $\alpha = 3.6$. Although the fit appears to be worse for models having $\alpha < 3.2$ or $\alpha > 3.9$, (or for the Gaussian model), the lower signal-to-noise ratios make the estimate of α rather imprecise.

Fig. 8 shows the 340-MHz data for PSR 1133+16. Here we feel B is only barely resolved. The model overplotted is for $\alpha = 3.6$, but comparable fits can be obtained for $3.4 < \alpha < 3.8$. The Gaussian model falls too steeply at large τ to give a good fit to the data.

As discussed earlier, some of the observations showed systematic drifting features in their frequency-time plots, particularly the high signal-to-noise pulsars in Figs 6, 7 and 8. Shishov (1974) has analysed how the drifts can be explained as refraction by irregularities which are too big to cause the scintillation fluctuations themselves. His equation (15) shows that the intensity correlation function versus frequency (at zero lag in time and space) is multiplied by an additional Gaussian function due to refraction. Thus $\tilde{\gamma}_4(\tau)$ is convolved with a Gaussian function whose width increases with increasing refraction. While we have not attempted to model this effect specifically, it is clear that the model curves of Figs 6, 7 and 8 would be broadened somewhat. However, the model curves would still fall off approximately exponentially at large τ and hence remain systematically below the observations at large τ.

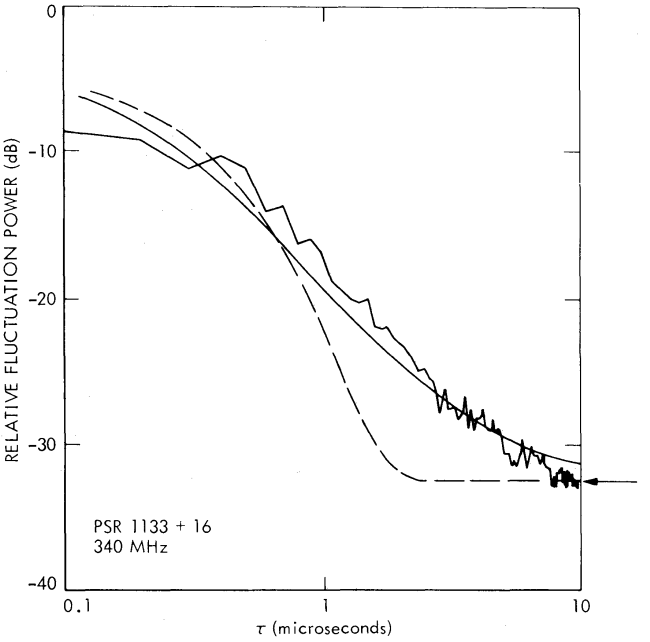

Figure 8. 'Fluctuation power spectrum', $\tilde{\gamma}_4(\tau)$, for PSR 1133+16. Centre frequency 340 MHz, 10-MHz rf bandwidth analysed. Overplotted model is the $\alpha = 3.6$ power law (solid line) and Gaussian model (dashed line).

5 Discussion

The results of our observations can be summarized as follows. When a correlation bandwidth is actually resolved, the observed scintillation indices are approximately unity (Table 1). When B is unresolved, m_{observed} is less than one, consistent with the idea that fluctuation 'scales' (in radio frequency) to which these observations were not sensitive could not contribute to the observed ISS variance. These scintillation-index results are not particularly surprising and do not exclude power-law models of the ISM. They do, however, constitute evidence for strong scattering ($U \gg 1$) for low DM, meter-wavelength measurements in a way that is observationally decoupled from intrinsic pulsar fluctuations. This is contrary to the suggestion of Bonazzola & Celnikier (1975). The scaling of B in dispersion measure (for $DM < 60\,\text{cm}^{-3}\,\text{pc}$) and radio frequency is also inconclusive in discriminating among the homogeneous power-law models considered here. The DM-scaling allows any $3.0 \lesssim \alpha \leqslant 4$ (or the Gaussian model) while the radio-frequency scaling for two pulsars allows α in the range 3.1–3.9 and 2.8–3.8, respectively. We have also demonstrated a method for comparing measured and model $\tilde{\gamma}_4$ shapes in the τ-domain. This method allows precise and relatively simple corrections for system noise and spectrometer resolution function, and is explicit in identifying the range of Fourier frequencies in the rf spectrum which is actually measured. Application of this method to our high signal-to-noise ratio data yields estimates of $4 > \alpha > 3.6$ (it should be noted that this method does not discriminate among models with slopes steeper than $\alpha = 4$). Thus, while analysis of the DM and radio-frequency dependences of correlation bandwidth would allow power-law models with α as low as 2.8, the 'steeper' power laws are required for consistency with the observed $\tilde{\gamma}_4$ shape.

The level of the ISM power spectrum required to give the observed correlation bandwidths can also be obtained. In light of our uncertainty in α, we adopt $\alpha = 11/3$ for this computation and use the method of Rickett (1977) (his equation 41). Obtaining distances from dispersion measures (using a density of $0.03\,\text{electron}\,\text{cm}^{-3}$) and ignoring the small

difference in definition of correlation bandwidth, we obtain estimates of the 'local' (< 1 kpc) C_N^2 in the range 3×10^{-5} to $3 \times 10^{-4}\,m^{-6.67}$. This is in good agreement with the values given by Rickett (1977) based on previous work. This then corresponds to the level of the three-dimensional power spectrum at wavenumber $q = 10^{-9}\,m^{-1}$ in the range 3×10^{28} to $3 \times 10^{29}\,m^{-3}$.

It is clear from our results that a spectrum of the power-law form fits the observations near a wavenumber of $10^{-9}\,m^{-1}$ somewhat better than a Gaussian spectrum. It seems likely that the spectrum proposed by Hall (1980) with a peak near $10^{-9}\,m^{-1}$ is incompatible with our results. Although we have not compared specific models of that form with our observations of $\tilde{\gamma}_4$, it seems clear that such spectra will give an even more 'convex' form to $\tilde{\gamma}_4$ than the Gaussian spectrum, which is already too convex to fit the data. Another argument favouring the range of scale sizes characteristic of a power-law spectrum is the link with large irregularities ($\gtrsim 10$ pc) known to exist in the interstellar medium (e.g. HI clouds and those causing Faraday rotation fluctuations; Jokipii & Lerche 1969; Jokipii 1974; Lee & Jokipii 1976). A power-law spectrum implies a hierarchy of intermediate scales. Shishov (1974) and Hewish (1980) also show that the scintillations drifting in frequency-time provide evidence of intermediate scales up to about 10^{11} m.

Further measurements of irregularities having scales between $\sim 10^9$ m and ~ 100 pc would clearly be desirable. One way this might be done is to measure time-of-arrival fluctuations of pulsar pulses caused by these intermediate-size irregularities drifting across the line-of-sight (Lovelace 1970; Rickett 1977). Such observations will be very difficult, however. Using $C_N^2 = 10^{-4}\,m^{-6.67}$, a transverse velocity of 200 km s^{-1}, and a typical distance through the medium of 1000 pc, we estimate $\Delta T_{rms} \sim 12\, T_{yr}^{5/6}\, \lambda_m^2\, \mu s$. Here T_{yr} is the extent of the timing observations in yr and λ_m is the observing wavelength in metres. To measure such a small effect and hence directly observe these intermediate scales would clearly require two-frequency data to separate the small, frequency-dependent scattering effect from the much larger intrinsic timing noise (Cordes & Helfand 1980).

Acknowledgments

We thank J. R. Fisher for valuable advice and help in setting up the observations. We have also benefited greatly from discussions with W. A. Coles, J. M. Cordes and S. R. Spangler. BJR thanks the Atmospheric Sciences Division of NSF for support under grant ATM 78-06770.

References

Armstrong, J. W., Spangler, S. R. & Hardee, P. E., 1977. *Astr. J.*, **82**, 785.
Bonazzola, S. & Celnikier, L. M., 1975. *Astr. Astrophys.*, **45**, 185.
Cesarsky, C. J., 1980. *A. Rev. Astr. Astrophys.*, 18, in press.
Chashei, I. V. & Shishov, V. I., 1976. *Soviet Astr.*, **20**, 13.
Condon, J. J. & Backer, D. C., 1975. *Astrophys. J.*, **197**, 31.
Condon, J. J. & Dennison, B., 1978. *Astrophys. J.*, **224**, 835.
Cordes, J. M. & Dickey, J. M., 1979. *Nature*, **281**, 24.
Cordes, J. M. & Helfand, D. J., 1980. *Astrophys. J.*, in press.
Hall, A. N., 1980. *Mon. Not. R. astr. Soc.*, **190**, 385.
Hewish, A., 1980. *Mon. Not. R. astr. Soc.*, **192**, 799.
Jenkins, G. M. & Watts, D. G., 1968. *Spectral Analysis and Its Applications*, Holden-Day, San Francisco.
Jokipii, J. R., 1974. Lecture presented at the summer school on Plasma Instabilities and Turbulence in Aix-en-Provence, France.
Jokipii, J. R. & Lerche, I., 1969. *Astrophys. J.*, **157**, 1137.
Lang, K. R., 1971. *Astrophys. J.*, **164**, 249.

Lee, L. C., 1974. *J. Math. Phys.*, **15**, 1431.
Lee, L. C. & Jokipii, J. R., 1975. *Astrophys. J.*, **201**, 532.
Lee, L. C. & Jokipii, J. R., 1976. *Astrophys. J.*, **206**, 735.
Lerche, I., 1979. *Astrophys. J.*, **234**, 262.
Lovelace, R. V. E., 1970. *PhD Thesis*, Cornell University.
Rankin, J. M., Comella, J. M., Craft, H. D. Jr., Richards, D. W., Campbell, D. B. & Counselman, C. C. III, 1970. *Astrophys. J.*, **162**, 707.
Rickett, B. J., 1970. *Mon. Not. R. astr. Soc.*, **150**, 67.
Rickett, B. J., 1977. *A. Rev. Astr. Astrophys.*, **15**, 505.
Roberts, J. A. & Ables, J. G., 1980. Preprint.
Rumsey, V. H., 1975. *Radio Sci.*, **10**, 107.
Shalloway, A. M., Mauzey, R. & Greenhalgh, J., 1972. *NRAO Electronics Division Internal Report No. 125.*
Shishov, V. I., 1974. *Soviet Astr.*, **17**, 598.
Sutton, J. M., 1971. *Mon. Not. R. astr. Soc.*, **155**, 51.
Taylor, J. H. & Manchester, R. N., 1975. *Astr. J.*, **80**, 794.
Woo, R. & Armstrong, J. W., 1979. *J. geophys. Res.*, **84**, 7288.

Appendix 1

In our comparison of the observed $\tilde{\gamma}_4$ curves with model predictions, we used theoretical results based on thin-screen scattering rather than extended-medium scattering. For the square-law structure function model, analytical results are available for both the thin-screen and the statistically homogeneous extended-medium cases (Chashei & Shishov 1976; Lerche 1979). For γ_4, the autocorrelation of the ISS in radio frequency, Chashei & Shishov (1976) obtain

$$\gamma_{4,s}(\Delta f) = \frac{1}{[1 + (2\pi t_D \Delta f)^2]}, \tag{A1.1}$$

$$\gamma_{4,e}(\Delta f) = \frac{2}{[\cosh\{(\sqrt{24}\ 2\pi\Delta f t_D)^{1/2}\} + \cos\{(\sqrt{24}\ 2\pi\Delta f t_D)^{1/2}\}]}, \tag{A1.2}$$

where the scale factor $\sqrt{24}$ has been introduced to make the asymptotic time constants of the Fourier transforms of the two expressions equal. Fig. 9 shows the Fourier transforms of $\gamma_{4,e}$ and $\gamma_{4,s}$. Clearly there is good agreement for time lags τ(cycle Hz^{-1}) greater than

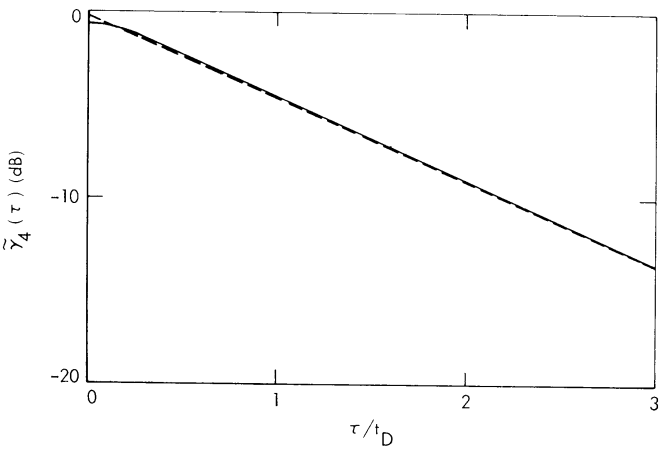

Figure 9. Comparison of thin screen and extended medium results for $\tilde{\gamma}_4(\tau)$ for the square-law structure function plotted on a log–linear scale. Solid curve is the extended-medium result of Chashei & Shishov (1976), dashed curve is thin-screen result. Both curves have the same area and the same exponential time constant at large τ. See Appendix 1.

about $0.3\,\tau_D$ where τ_D is the asymptotic time constant for $\tilde{\gamma}_{4,s}$. This suggests that the use of extended-medium calculations for γ_4, versus the thin-screen calculations used here, would not lead to strongly different conclusions.

Appendix 2

The quotient spectrum $I(\omega)$ is a set of estimates of the intensity averaged over some time interval (30–60 s) and over the spectrometer resolution function $R(\omega)$. Thus $I(\omega) = I'(\omega) * R(\omega)$, whre $I'(\omega)$ is the product of the pulsar spectrum and the ISS spectrum at that time. (Here an asterisk denotes convolution.) We assume that the averaged pulsar spectrum is flat over our bandwidths and thus that the quantity of principal interest is $\gamma_4'(\Delta\omega) = \langle I'(\omega) \cdot I'(\omega + \Delta\omega)\rangle$. This is related to $\gamma_4(\Delta\omega)$, the autocorrelation of the observed $I(\omega)$, by $\gamma_4(\Delta\omega) = \gamma_4'(\Delta\omega) * \int R(\omega) \cdot R(\omega + \Delta\omega)\, d\omega$. In the transform domain we get $\tilde{\gamma}_4(\tau) = \tilde{\gamma}_4'(\tau) \cdot |\tilde{R}(\tau)|^2$. For our observations $R(\omega) = \sin(\pi\omega/\delta\omega)/(\pi\omega/\delta\omega)$; hence $|\tilde{R}(\tau)|^2$ is a rectangle of width $\pm\tau_n = \pm\pi/\delta\omega$, where $\delta\omega$ is the 'width' of the resolution function. Consequently, we can ignore the effect of the resolution function out to τ_n and $\tilde{\gamma}_4(\tau) = \tilde{\gamma}_4'(\tau)$. The corresponding estimate of $\gamma_4(\Delta\omega)$ is smoothed by the resolution function $R(\omega)$ over an interval of $\delta\omega$.